CrossMark

ORIGINAL PAPER

The choroid plexus is a key cerebral invasion route for T cells after stroke

Gemma Llovera[1,2] · Corinne Benakis[1] · Gaby Enzmann[3] · Ruiyao Cai[1,2] · Thomas Arzberger[4,5] ·
Alireza Ghasemigharagoz[1] · Xiang Mao[1] · Rainer Malik[1] · Ivana Lazarevic[3] · Sabine Liebscher[2,6] · Ali Ertürk[1,2] ·
Lilja Meissner[1] · Denis Vivien[7] · Christof Haffner[1] · Nikolaus Plesnila[1,2] · Joan Montaner[8] · Britta Engelhardt[3] ·
Arthur Liesz[1,2]

Abstract Neuroinflammation contributes substantially to stroke pathophysiology. Cerebral invasion of peripheral leukocytes—particularly T cells—has been shown to be a key event promoting inflammatory tissue damage after stroke. While previous research has focused on the vascular invasion of T cells into the ischemic brain, the choroid plexus (ChP) as an alternative cerebral T-cell invasion route after stroke has not been investigated. We here report specific accumulation of T cells in the peri-infarct cortex and detection of T cells as the predominant population in the ipsilateral ChP in mice as well as in human post-stroke autopsy samples. T-cell migration from the ChP to the peri-infarct cortex was confirmed by in vivo cell tracking of photoactivated T cells. In turn, significantly less T cells invaded the ischemic brain after photothrombotic lesion of the ipsilateral ChP and in a stroke model encompassing ChP ischemia. We

detected a gradient of CCR2 ligands as the potential driving force and characterized the neuroanatomical pathway for the intracerebral migration. In summary, our study demonstrates that the ChP is a key invasion route for post-stroke cerebral T-cell invasion and describes a CCR2-ligand gradient between cortex and ChP as the potential driving mechanism for this invasion route.

Introduction

Ischemic stroke remains one of the main causes of death and disability in the world with only very limited therapeutic options [10]. Over the past decade, post-ischemic neuroinflammation in secondary neuronal loss and repair after stroke has come into the focus of preclinical stroke research [14, 25]. Invasion of circulating, pro-inflammatory lymphocytes has been described as the key mechanism of the post-ischemic neuroinflammatory response, which aggravates the

✉ Arthur Liesz
Arthur.Liesz@med.uni-muenchen.de

1 Institute for Stroke and Dementia Research, Klinikum der Universität München, Feodor-Lynen-Str. 17, 81377 Munich, Germany

2 Munich Cluster for Systems Neurology (SyNergy), Munich, Germany

3 Theodor Kocher Institute, University of Bern, Freiestrasse 1, 3012 Bern, Switzerland

4 Center for Neuropathology and Prion Research, Ludwig-Maximilians-Universität, Feodor-Lynen-Str. 23, 81377 Munich, Germany

5 Department of Psychiatry and Psychotherapy, Ludwig-Maximilians-Universität, Nussbaumstraße 7, 80336 Munich, Germany

6 Institute of Clinical Neuroimmunology, Klinikum der Universität München, Ludwig-Maximilians-University, Grosshaderner Str. 9, 82152 Munich, Germany

7 INSERM, UMR-S U919, Institut National de la Santé Et de la Recherche Médicale (INSERM), Team Serine Proteases and Pathophysiology of the Neurovascular Unit, GIP CYCERON, University Caen Basse-Normandie, 14074 Caen Cedex, France

8 Neurovascular Research Laboratory, Vall d'Hebron Research Institute (VHIR), Universitat Autònoma de Barcelona, Barcelona, Spain

initial infarct volume and exacerbates stroke outcome [4, 24]. Recent experimental studies demonstrated that amelioration of cerebral lymphocyte invasion by reducing the number of circulating lymphocytes in different experimental stroke models improved functional outcome [1, 18, 26, 31]. In parallel, first clinical trials have been initiated which tested this treatment approach in stroke patients using two drugs currently approved for multiple sclerosis, fingolimod (FTY720) and natalizumab (humanized anti-α4-integrin IgG4). Even though the early translation of immune-targeted therapies in stroke and the first positive results are very promising, these attempts have also been criticized as premature in face of several unsolved key questions in the field of stroke immunology [9, 39]. One of these main unresolved questions in the field is the exact mechanism of lymphocyte migration into the ischemic brain. In stroke research, the vascular migration route across the (damaged) blood–brain barrier (BBB) has been assumed as the main invasion route for circulating lymphocytes into the ischemic brain [41]. Although other infiltration routes such as meningeal blood vessels or the choroid plexus (ChP) have previously been characterized as important entry sites of lymphocytes in primary inflammatory brain disorders such as experimental autoimmune encephalitis (EAE) [30, 45], these alternative invasion sites have not been analyzed in post-stroke neuroinflammation.

Therefore, in the present study, we aimed to investigate the role of the ChP as a potential infiltration route for lymphocytes—particularly pro-inflammatory T cells—into the post-ischemic brain. We particularly focused on the ChP as an infiltration route for T cell due to the key pathophysiological role of T cells in post-stroke neuroinflammation and a specific invasion pattern observed for T cells in contrast to myeloid cells. We observed that a large proportion of brain-invading T cells migrate through the ChP after stroke. Moreover, we could identify the CCR2-dependent pathway as a key chemoattractant signal for T cells along the choroidal infiltration route.

Materials and methods

Mice

All experiments were conducted in accordance with national guidelines for the use of experimental animals, and all protocols were approved by the German governmental committees (Regierung von Oberbayern, Munich, Germany). 83 wild-type male C57BL6/J mice were obtained from Charles River. 17 *Rag1*$^{-/-}$ (B6.129S7-Rag1$^{tm1Mom/J}$), 10 *CAG-EGFP* (C57BL/6-Tg (CAG-EGFP)131$^{osb/LeySopJ}$), 22 heterozygous *PA-UBC-GFP* (B6.Cg-Ptprc Tg (UBC-PA-GFP)1$^{Mnz/J}$), 5 *CCL2-RFP* (B6.Cg-*Ccl2tm1.1*$^{Pamel/J}$) and 5 *CCL2*$^{-/-}$ (B6.129S4-*Ccl2tm1*$^{Rol/J}$) male mice were

obtained from Jackson Laboratories (USA). Eight female *LysM-eGFP* (Lyz2tm1.1^{Graf}) mice were kindly donated by M.Sperandio (Walter BrendlCenter for Experimental Research, Munich, Germany). CCR2$^{RFP/RFP}$CX3CR1$^{GFP/+}$ and CCR2$^{RFP/+}$CX3CR1$^{GFP/+}$ mice were originally generated by Israel Charo and Richard Ransohoff [32] and bred at the Theodor Kocher Institute, University of Bern, Switzerland. All other animals were housed at the core animal facility of the Institute for Stroke and Dementia Research, Munich, under controlled temperature (22 ± 2 °C), with a 12-h light–dark cycle period and had access to pelleted food and water ad libitum. All animals used for this study were at 8–12 weeks of age, expect for the aged mice which were 8 months old. Number of excluded animals from each experiment is shown in Suppl. Table 1.

Human samples

Both lateral ventricles with surrounding brain tissue from five stroke and six control human patients were obtained from the Human Brain and Spinal Fluid Resource Center (HBSFRC) Los Angeles, USA. Patient characteristics are described in Suppl. Table 2. Samples were sent frozen to our facility where they were kept at −80 °C until used. Samples were slowly defrosted at 4 °C for 3 h and then fixed in 4% paraformaldehyde (PFA) (pH 7.4) for 1 h at 4 °C and afterwards at room temperature (RT) for 48 h in the dark. After parafinization, 5 μm thick sections were cut for histology and immunohistochemistry. For conventional histological investigations, hematoxylin–eosin (H&E) stains were performed. Immunohistochemistry for CD3 (rabbit polyclonal, A0452/DAKO, diluted 1:50) or CD68 (mouse clone KP1, M0814/DAKO, diluted 1:50) was done in a Ventana Benchmark GX using the i-View detection system and diaminobenzidine as chromogen following the instructions of the manufacturer. Counterstaining was done with hematoxylin. ChP samples were analyzed under a microscope (Axio ImagerM2, Zeiss) and each CD3- and CD68-positive cell was counted. Total cell count per staining and per sample was normalized to the ChP area which was manually determined on H&E-stained sections.

Human RNA samples from six patients were obtained from the Hospital de la Vall d´Hebron, Barcelona. Patient characteristics are described in Suppl. Table 3. RNA from the ipsilateral and contralateral cortex of each patient was isolated using the Speed tools total RNA extraction kit (21.211, Biotools). 20 μl of total RNA was hybridized with reporter and capture probes in human nCounter gene expression code sets GX Human Immunology Kit V2 (XT-SC-HIM2-12) according to manufacturer's instruction (NanoString Technologies). Data were analyzed using nSolver Analysis software. Additional analysis was performed using "NanoStringNorm" in R (version 3.3.1) [43].

The geometric mean was used to summarize the CodeCount (positive) and SampleContent (housekeeping genes) controls, thus minimizing the impact of outliers. Stringent background correction was applied (mean + 2 standard deviations) to minimize false positives and therefore increasing specificity. As an additional QC step, housekeeping genes with high variability (SD >2) were removed before normalizing the data.

Permanent middle cerebral artery occlusion (pMCAo) model

As previously described [21], animals were anesthetized with volatile anesthesia (isoflurane in 30%O_2/70%N_2O) and placed in lateral position. After a skin incision between eye and ear, the temporal muscle was removed and the MCA identified. Then, a burr hole was drilled over the MCA and the dura mater was removed. The MCA was permanently occluded using bipolar electrocoagulation forceps. Permanent occlusion of the MCA was visually verified before suturing the wound. During the surgery, body temperature was maintained using a feedback-controlled heating pad. Mice that developed a subarachnoid hemorrhage during surgery were excluded from the analysis.

Transient middle cerebral artery occlusion (fMCAo) model

Animals were anesthetized (isoflurane in 30%O_2/70%N_2O, local lidocaine) and received an incision between ear and eye to expose the temporal skull. A laser Doppler probe was placed over on the skull above the MCA territory. Animals were then placed in supine position. After a midline neck incision, the common carotid artery and left external carotid artery were isolated and ligated, a 5 mm silicon-coated filament (Doccol, #7019PK5Re) was inserted into the internal carotid artery and MCA occlusion checked by a corresponding laser Doppler flow reduction. After 90-min MCAo, animals were anesthetized again and the filament was removed. For the survival period, animals were kept in their home cage with facilitated access to water and food. Mice without a reduction in blood flow to <20% of the baseline, controlled by a laser Doppler flow, were excluded from the analysis.

Photothrombosis (cortical and choroid plexus lesion)

Animals were placed in a stereotactic device under anesthesia (isoflurane in 30%O_2/70%N_2O).

For ChP lesions, a midline incision was performed to expose the skull and both bregma and Lambda points were identified. A burr hole was drilled at 3 mm anterior from bregma, 1 mm left from midline. Animals then received 10 μl/g body weight (BW) of 1% Rose Bengal in phosphate buffer saline (PBS) intraperitoneally (i.p). and after 5 min an optical fiber with an inner diameter of 200 μm and a NA of 0.22 was inserted at 4 mm depth from the brain surface to reach the left ventricle with an inclination angle of 30°. Photothrombosis of the ChP was achieved by 15 min illumination via the fiber probe at 532 nm wavelength (Luxivision, Germany). Control animals received the same treatment with saline injection instead of the Rose Bengal administration, including illumination of the lateral ventricle.

For cortical lesions, after midline incision and skull exposure, a laser (Cobolt HS-03, Solna, Sweden) was centered at 4 mm lateral to bregma on the left side. A fiber optic bundle of 1.5 mm diameter at the tip was used to obtain a stroke lesion similar to that induced by the pMCAo model. Animals then received 10 μl/g body weight of 1% Rose Bengal in PBS i.p. and after 5 min the brain was illuminated through the intact skull for 15 min at constant 561 nm wavelength.

Traumatic brain injury

Traumatic brain injury (TBI) was induced as previously described [34]. Briefly, mice were anesthetized with a gas mixture containing 2% isoflurane, 65% N_2O, and 33% O_2. A craniotomy window was drilled over the right parietal cortex under continuous cooling with saline. A cortical contusion was produced using a controlled cortical impact device optimized for use in mice (cylinder diameter 3.0 mm; velocity 6.0 m/s; penetration depth 0.5 mm; contact time 150 ms). Immediately following the impact, the bone flap was reimplanted and fixed using histoacrylic glue. The animals were then allowed to wake in a recovery chamber (33 °C and 50% humidity) and killed 5 days post-injury.

Assessment of infarct volume

Mice were deeply anesthetized 5 days after stroke induction and transcardially perfused with 10 ml saline. Brains were removed, frozen immediately on powdered dry ice and stored at −20 °C. For infarct volumetry, brains were serially sectioned (400 μm intervals, 20 μm thick) and stained for cresyl violet (CV) as previously described [21]. CV-stained sections were scanned at 600 dpi on a flatbed scanner (Canon). For the pMCAo and PT model, direct infarct measurement was used after validating the absence of edema at the investigated time point (5 days after pMCAo or PT). The total infarct volume was measured with ImageJ and determined by integrating measured areas and distances between sections.

Intraventricular matrigel injection

Immediately after pMCAo, animals were prepared as described above for the photothrombosis procedure.

Specifically, a 10 µl Hamilton syringe with a 10 mm length needle (Hamilton, #7804-03) was introduced into the lateral ventricle at an inclination angle of 30°. For the CSF blockage, 6 µl of matrigel (BD Matrigel™ Matrix, BD Biosciences, #354230) was injected over 5 min. Matrigel was kept at 12 °C in a cooling block until the time of injection, in order to prevent its polymerization. 5 days after pMCAo and matrigel injection, mice were transcardially perfused with 10 ml saline and 10 ml 4% PFA. For the visualization of the matrigel into the ventricle, 5 µl of matrigel + 1 µl of Evans Blue was injected in 5 min, 24 h after the injection mice were killed, brain was cut and immediately visualized under a microscope.

Immunohistology

Mice were transcardially perfused at the indicated time points with 10 ml saline and 10 ml 4% PFA (pH 7.4), then post-fixed in 4% PFA for 4 or 24 h for *PA-UBC-GFP* animals at 4 °C and immersed with 30% sucrose in PBS, then brains were frozen in −20 °C isopentane. 12 µm thick coronal sections were obtained at the level of anterior commissure for immunohistochemical analysis. Sections were mounted on SuperfrostPlus Slides (Thermo Scientific) and stored at −80 °C. Then sections were dried at room temperature for 1 h. After washing with PBS, slides were fixed with acetone at −20 °C for 5 min, this was followed by washing with PBS and PBS containing 0.1% Triton and incubation in blocking buffer containing 0.1% Triton, 0.05% Tween20, 1% bovine serum albumin, 0.1% cold fish skin gelatine and 2% goat serum in PBS at RT for 1 h before overnight incubation at 4 °C with the primary rabbit anti-CD3 antibody (1:50, abcam #16669), rat anti-CD4 antibody (clone GK1.5, 1:200, Abcam), chicken anti-laminin (1:200, Abcam) or mouse anti-CD45 (1:100, clone 104-2, Abcam) and labeled for 1 h with the secondary antibody AF594 goat anti-rabbit (1:200, Invitrogen), Cy3 goat anti-rat IgG + IgM (H + L) (1:200, Jackson Immunoresearch), FITC anti-chicken Ig H& <l (1:200, Abcam) or AF488 goat anti-mouse IgG (H + L) (1:100, Invitrogen). Finally, sections were stained with DAPI and mounted with fluoromount medium (Sigma). Samples were analyzed on an epifluorescence microscope (Zeiss Axiovert 200 M) or a confocal microscope (Zeiss 880). CD3+ cells were counted on one 12 µm section per brain at bregma or on three consecutive 12 µm sections at bregma ±60 µm for *PA-UBC-GFP* animals. The infarct core was delimited on consecutive CV-stained sections for each individual animal. Only cells at the outer border of this area (peri-infarct region) were included for quantification analysis. The localization of each single CD3$^+$ and CD45$^+$ was marked on a topographic map according to the mouse brain atlas to achieve cumulative localization maps.

For the ChP cell death analysis: 24 h after pMCAo and fMCAo, mice were perfused with 10 ml saline and brains were removed, placed in cold PBS and the ChP from both lateral ventricles were isolated. Apoptotic cell death was detected by terminal deoxy-nucleotidyl-transferase-mediated dUTP nick-end labeling (TUNEL) according to the manufacturer's instructions (Millipore). 20-µm thick coronal sections were stained with the TUNEL kit to verify cell death in the brain.

Flow cytometry

After perfusion with saline, the ChP was removed under a stereomicroscope (Leica) and collected in 200 µl Dulbecco's Modified Eagle Medium (DMEM) + 10% fetal calf serum (FCS). ChP cells were isolated by incubating the samples in 2 ml of digestion mix [DMEM + 10% FCS + 0.4% DNASEI (#11284932001, Roche) + 3% CollagenaseD (#11088866001, Roche)], 10 min at 37 °C, and then mechanically dissociated. Brain homogenates of both hemispheres were prepared by the same dissociation/digestion protocol. Cerebral mononuclear cells were subsequently isolated using a 70 and 40% discontinuous Ficoll gradient. The following mouse antigen-specific antibodies were purchased from eBioscience: CD45 eF450 (30-F11), CD11b PE-Cy7 (M1/70), CD3 V510 or FITC (17A2), CD19 APC-Cy7 (eBisID3), CD8 PE (53-6.7), CD4 PerCP5.5 (45-0042-82), Ly6C APC (HK1.4), Ly6G PE Cy7 (RB6-8C5) and Ly6G PE (1A8). To quantify the various cell populations, cells were stained with specific antibodies in accordance with the manufacturer's protocols, acquired in a FACSVerse flow cytometer and analyzed with FlowJo software (version 10, Tree Star).

Adoptive T-cell transfer

Spleen and mesenteric lymph nodes from *CAG-eGFP* mice were isolated under sterile conditions and kept in MACS buffer (PBS + 0.5% BSA + 2 mM EDTA). After preparing a single cell suspension, T cells were isolated using a mouse T-cell enrichment kit (eBioscience). *Rag1$^{-/-}$* mice received 10^6 T cells in 500 µl PBS i.p. Stroke induction was performed 7 days after the T-cell transfer to allow expansion of T cells in the recipient mice.

Clearing and light-sheet microscopy

For visualization of the T-cell invasion pattern, mice were perfused transcardially with 10 ml saline and 10 ml 4% PFA (pH 7.4) 5 days after pMCAo induction in *Rag1$^{-/-}$* mice receiving adoptive (eGFP+) T-cell transfer. For the study of the neuroanatomical structure of the ChP of lateral ventricles, mice were perfused with lectin-FITC in normal saline. Then mice were perfused

transcardially with 10 ml saline and 10 ml 4% PFA (pH 7.4). Whole brains were cleared using uDISCO protocol [28]: first, they were serially incubated in *tert*-butanol in 12 h until overnight incubation in 100% *tert*-butanol. The next day, samples were incubated for 1 h and 30 min in dichloromethane and finally incubated in refractive index matching solution BABB-D15, prepared by mixing BABB (benzyl alcohol + benzyl benzoate 1:2) with diphenyl ether (DPE) at a ratio of 15:1 and adding 0.4% vol DL-alpha-tocopherol (Vitamin E), for at least 4 h until the samples became transparent. Next, samples were imaged by a light-sheet microscope (LaVision BioTec). Images were acquired with a z-step of 4–8 µm, using 50 ms as exposure time and tiling scans to cover the entire specimen. Images obtained by light-sheet microscopy were analyzed by Amira software (version 6) for segmentation and 3D reconstruction. Due to uneven light penetration through the sample, we equalized raw image stacks using the pseudo flat-field correction method with the BioVoxxel plugin in Fiji software. The infarct core was segmented manually for exclusion from further analyses. T cells were segmented as individual cells for illustration using a 1.7-fold ratio of the transcellular fluorescence intensity profile peak over the neighboring tissue background fluorescence. This threshold was determined using manual identification of cells based on size, shape and peak signal intensity. No additional autofluorescence correction or background subtraction was performed.

In vivo photoactivation

Animals were prepared as described above for the photothrombosis procedure including insertion of an optical fiber into the lateral ventricle at an inclination angle of 30°. For the in vivo "pulse-chase experiment": photoactivation was performed for 5 min with a laser source of 405 nm wavelength (Luxivision, Germany) with an effective output power at the tip of the fiber of 5 mW. For 24-h photoactivation in freely behaving mice: immediately after pMCAo a burr hole was drilled under isoflurane anesthesia 3 mm anterior from bregma, 1 mm left from midline. Then a mono fiberoptic cannula with an inner diameter of 200 µm, a NA of 0.22 and 4 mm length was inserted into the left lateral ventricle with an inclination angle of 30° and fixed with dental cement (Cyano Veneer, Hager Werken). In another set of experiments, photoactivation was performed 4 days after pMCAo for 24 h at constant 405 nm illumination. Mice were then transcardially perfused with 10 ml saline and 10 ml 4% PFA. PA-GFP$^+$ and PA-GFP$^-$ cells were quantified on coronal sections. Percentage of infiltrated T cells shown in Fig. 2h was calculated as follows: [(T cells at 5 days − T cells at 4 days)/total T cells at 5 days] × 100].

RT-PCR array

Four 100 µm thick brain cryosections from naïve animals and 24 h pMCAo animals were collected into a MembraneSlides 1.0 Pen (Zeiss). Microbeam laser microdissection (Zeiss) was used to cut the ChP and peri-infarct cortex (880 µm × 620 µm) of the sections. Microdissected tissue was carefully placed with sterile forceps into a 0.5 ml sterile sample tube. Arcturus-PicoPure RNA Isolation Kit (Applied Biosystems) was used for RNA extraction and RT^{2}PreAMPcDNA syntesis Kit (Qiagen) was used for the cDNA synthesis. Finally, a RT2 Profiler PCR Array for chemokines and chemokine receptors (PAMM-022Z, Qiagen) was run on a Roche LightCycler 480 following the manufacturer's instructions. Data were analyzed with RT^2 Profiler PCR Array Data analysis software (version3.5) from SABiosciences.

Histological CCL2 gradient analysis

24 h after pMCAo induction in *CCL2-RFP* reporter mice, animals were prepared as described above for immunohistological analyses. A mosaic picture from a 12 µm coronal section at bregma level was obtained with a confocal microscope (Zeiss 880) (40× magnification), producing 346 regions of interest (ROI). Mean RFP signal per individual ROI from each individual z-stack was analyzed by the thresholding technique using ImageJ software. Following this, RFP values were rasterized from each ROI, and normalized to the range between 1.0 and 10.0, representing 1.0 the lowest and 10.0 the highest RFP expression. Each ipsilateral ROI was subsequently normalized to the anatomically homotypical ROI of the contralateral hemisphere to normalize for unspecific background fluorescence.

Statistical analysis

Data were analyzed using GraphPad Prism (version 6.0). Summary data are expressed as the mean ± standard deviation (SD) or mean ± standard error of the mean (SEM). All data sets were tested for normality using the Shapiro–Wilk normality test. The groups containing normally distributed data were tested using a two-way Student's *t* test (for 2 groups) or ANOVA (for >2 groups). The remaining data were analyzed using the Mann–Whitney *U* test. Differences with a *p* value <0.05 (or <0.1 for the PCR array) were considered to be statistically significant.

Results

The invasion patterns of myeloid and T cells differ after stroke

We investigated the regional distribution pattern of myeloid and T cells in a focal, cortical ischemia model in mice by
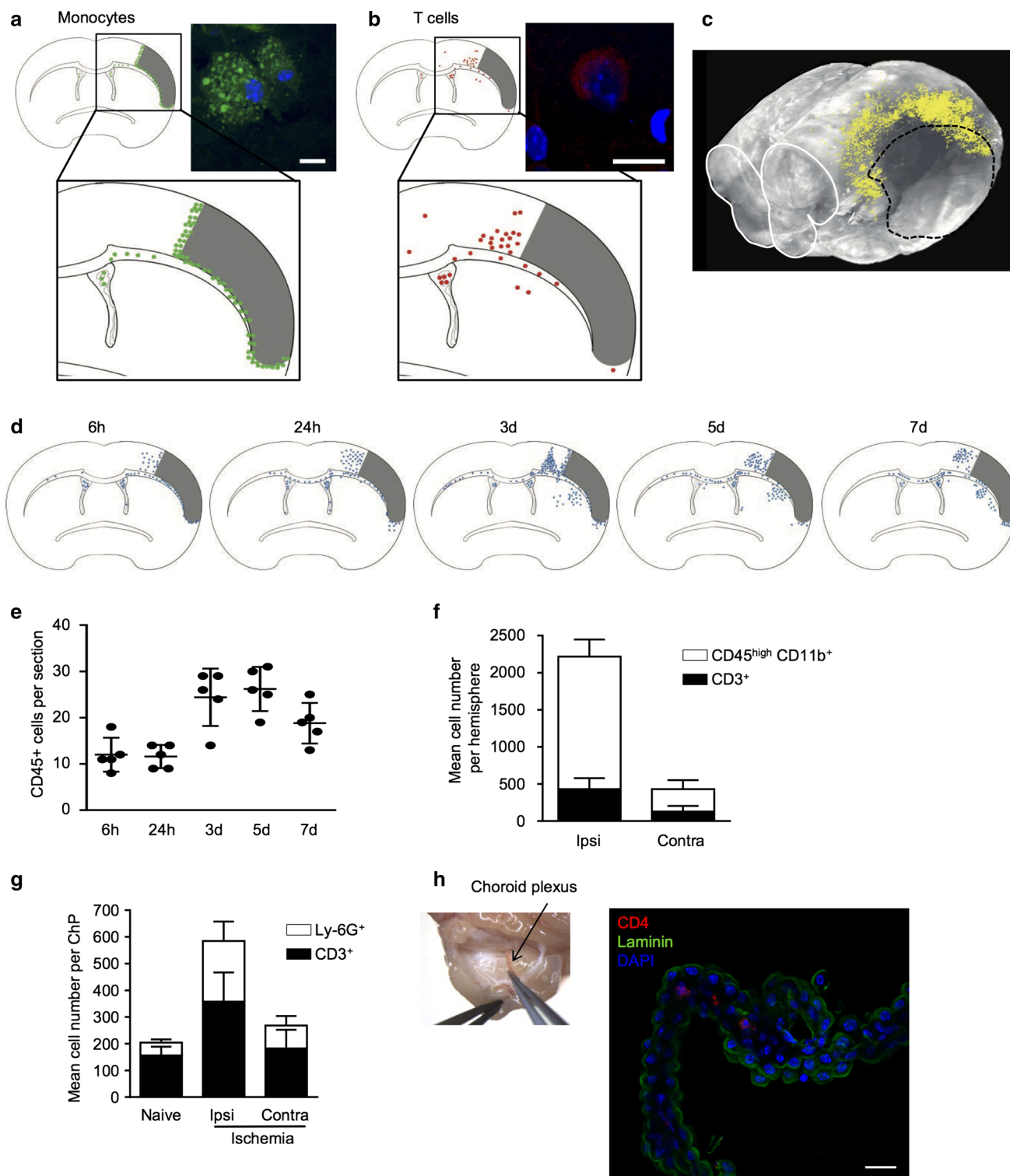
permanent occlusion of the distal middle cerebral artery (pMCAo). Cerebral T cells where visualized by immunohistological staining and myeloid cells by *LysM-eGFP* reporter mice. The ischemic core itself was excluded from this and any subsequent analyses, as we focused on the role of invading leukocytes to secondary mechanisms in the surrounding tissue at risk rather than the already necrotic infarct tissue, which undergoes later liquefaction. 5 days after stroke induction—which was the time point of maximum cerebral leukocyte invasion in this model (Fig. 1d, e)—we observed LysM-eGFP-positive myeloid cells to uniformly surround the ischemic core (Fig. 1a). In contrast, analysis of regional

◄**Fig. 1** Lymphocytes display a distinct cerebral invasion pattern. Accumulative topographic representation of each single **a** myeloid cell (*inset*: *green* LysM-eGFP+ myeloid cells, *blue* nuclear DAPI stain) and **b** CD3+ T cell (*inset*: *red* CD3+ T cell, *blue* nuclear DAPI stain) 5 days after permanent MCA occlusion (pMCAo). Cells were accumulated from one section at bregma level of five animals each. The infarct is depicted in *gray*. *Scale bar* 10 μm. **c** T-cell segmentation and 3D reconstruction after brain clearing of 5 days post-lesion of transferred eGFP + T cells to lymphocyte-deficient *Rag1−/−* mice revealed specific T-cell distribution (*yellow dots*) in the peri-infarct cortex between the ipsilateral ventricle and the lesion 5 days after pMCAo. The *dashed line* demarcates the infarct core. **d** Corresponding cumulative topographic maps of CD45+ leukocytes at the indicated time points after stroke. Cells were accumulated from one section at bregma level of five animals each. Each cell is represented as a *single dot*. The infarct is depicted in *gray*. **e** Quantification of total leukocytes at the indicated time points after pMCAo, indicating the peak of the infiltrated cells at 5 days after pMCAo. Comparative analysis are represented as mean ± SD. **f** Flow cytometric analysis showing the absolute number of myeloid cells (CD45+CD11b+) and T cells (CD3+) in the ipsilateral ischemic (Ipsi) and contralateral (Contra) brain hemispheres 5 days after pMCAO. **g** Myeloid cells (CD45^{high} CD11b+) cells and T cell (CD3+) ratios in ChP 5 days after pMCAO were substantially different between the ipsi- and contralateral ChP after stroke as well as an increased cellularity of the ipsilateral ChP was observed after stroke compared to a naïve ChP (*n* = 10–18, 3 individual experiments). Data are presented as mean ± SEM **h** *left*, photograph showing the ChP located in the lateral ventricle 5 days after stroke. *Right* representative image demonstrating T-cell (CD4+) accumulation in ChP 5 days after stroke. *Scale bar* 20 μm

T-cell distribution revealed a completely different invasion pattern with T cells predominantly clustering in the peri-infarct cortex between the lateral ventricle and the lesion site (Fig. 1b). To better visualize this serendipitous observation of a specific T-cell distribution pattern, we performed 3D light-sheet microscopy of uDISCO solvent-cleared brains [28]. For this analysis, we adoptively transferred eGFP + T cells to lymphocyte-deficient *Rag1−/−* mice. Seven days later, we induced the stroke lesion and at 5 days post-lesion performed clearing and imaging of whole brains by light-sheet microscopy. Thereby, we were able to confirm 3-dimensional T-cell invasion clustering as a "wave front" in the peri-infarct cortex between the lateral ventricle and cortical infarct core (Fig. 1c). This obvious difference in the invasion pattern between T cells and myeloid cells prompted us to further investigate potential differences in cerebral migratory pathways between leukocyte subsets. We performed a quantification of myeloid cells and T-cell counts in the brain parenchyma and ChP by flow cytometry. As expected, both populations, myeloid cells (CD45^{high}CD11b+) and T cells (CD3+), were increased in the ipsilateral compared to the contralateral hemisphere after stroke. The total cell number of myeloid cells was substantially higher than of T cells in the parenchyma (Fig. 1f). In contrast to the brain parenchyma, cellular distribution of leukocyte subpopulations differed in the ChP isolated from both lateral ventricles. Flow

cytometric analysis revealed a surprisingly high absolute cell numbers of T cells in the ChP (Fig. 1g), which we were able to confirm by histological staining demonstrating accumulation of T cells in the ChP stroma (Fig. 1h). To test whether the specific clustering of T cells in the peri-infarct cortex is merely a model-dependent effect after pMCAo surgeries or a distinct feature attributable to specific mechanisms of post-stroke T-cell invasion, we analyzed regional T-cell distribution in an independent cortical infarct model. We induced photothrombosis (PT) of the cortex through the intact skull without any surgical manipulation at the skull or intracerebral structures, resulting in ischemic lesions of similar shape and location as pMCAo (Suppl. Figure 1). Although the infarct volume was smaller in the PT model, we detected a comparable cerebral T-cell invasion pattern with peri-infarct cortical T-cell clustering and with similar absolute cell counts per histological section as in the pMCAo model. Additionally, we could confirm a similar T-cell invasion pattern also in a third independent model of cortical injury: mild TBI and finally, also after pMCAo in aged animals (Suppl. Figure 1). These results confirmed a previously unrecognized and specific invasion pattern of T cells after cortical infarction in the different acute brain injury models tested. Considering the differences in regional invasion patterns and relative abundance in the ChP between monocytes and T cells, these results indicated a potentially specific role of the ChP for cerebral invasion of T cells after stroke.

The choroid plexus is a primary entry site for T cells into the ischemic brain

Based on these descriptive results, we next aimed to investigate specifically the intracerebral migration of T cells from the ChP to the peri-ischemic cortex after stroke. To this end, we used transgenic *UBC-PA-GFP* mice expressing photoactivatable (PA)-GFP in T cells, in which illumination at 405 nm results in a stable shift in the peak excitation wavelength with a half-life of approximately 30 h [42]. This model enabled us to perform an in vivo "pulse-chase experiment" with labeling of T cells within one lateral ventricle with high anatomical precision. Four days after pMCAo, a 40 μm thin laser fiber was introduced into the ipsilateral ventricle and illuminated at a wavelength of 405 nm for 5 min (Fig. 2a), then animals were killed at different time points after the illumination and histologically analyzed for the localization of GFP-positive/-negative T cells stained for CD3+ (Fig. 2b). This validation of T-cell-specific photoactivation was necessary due to the potential expression of PA-GFP also in other hematopoietic cell populations, which was, however, not observed in this model. We detected photoactivated T cells (CD3+ PA-GFP+) in the peri-infarct cortex as early
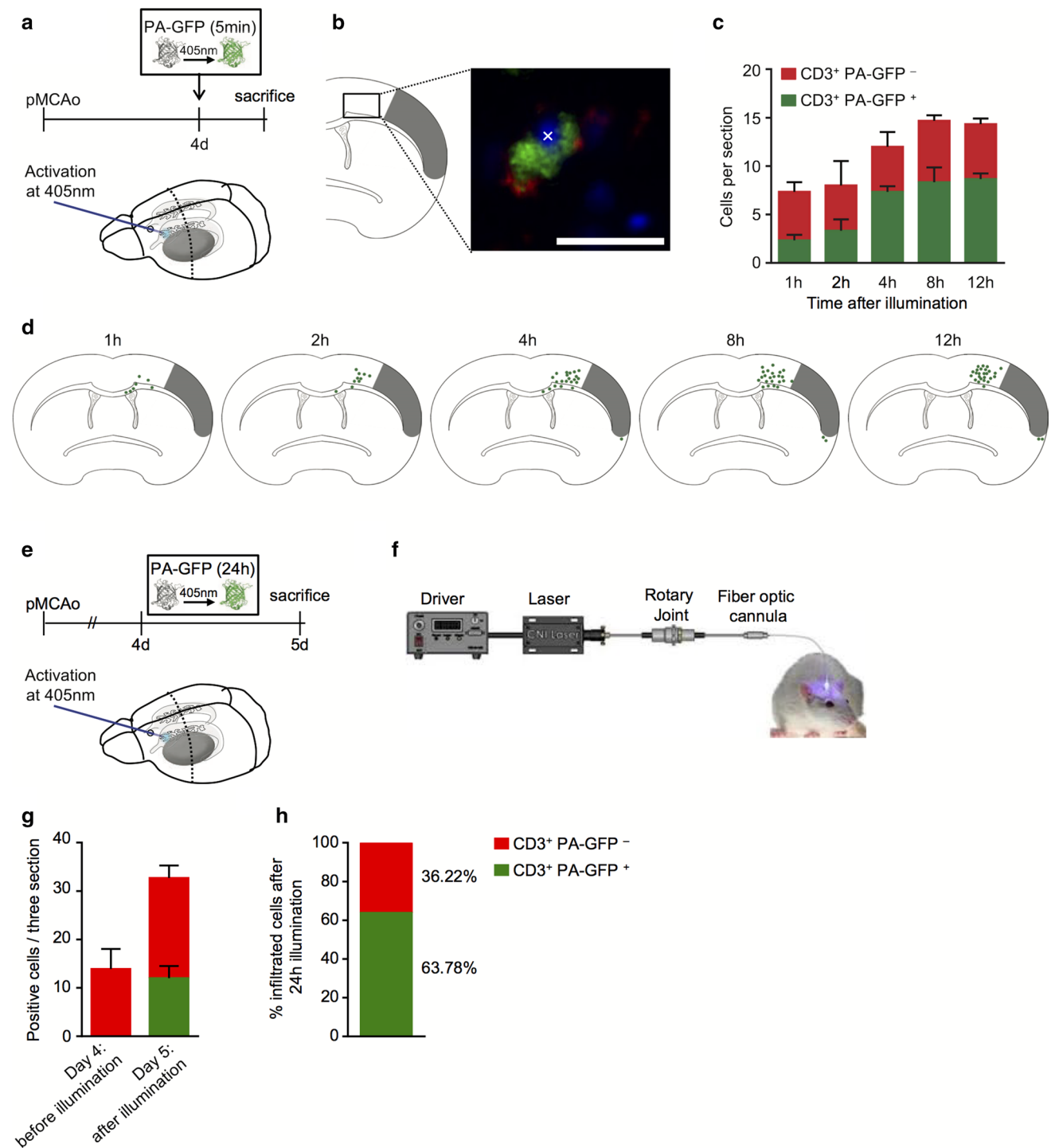
as 1 h after illumination and the number of photoactivated T cells peaked and reached a plateau at 8 h after intraventricular illumination (Fig. 2c, d). These results demonstrate a directed intracerebral migration of T cells from the ChP of the ipsilateral ventricle to the peri-infarct cortex after stroke. Importantly, as a control experiment, we did not observe photoconverted cells in the brain

parenchyma at the proximity of the ventricle 24 h after inducing illumination in the ventricle (Suppl. Figure 3). Interestingly, at early time points after intraventricular illumination photoactivated T cells were located in the corpus callosum while at later time points, GFP-positive T cells were mainly detected in the cortex (Fig. 2c, d). This shift in the photoactivated T-cell localization suggests an

◄**Fig. 2** T cells migrate from the ChP to the peri-infarct cortex. **a** Schematic illustration of the experimental design to perform intraventricular/ChP optical labeling of T cells for an "in vivo pulse-chase" experiment of intracerebral T-cell migration. **b** Representative picture of photoactivated PA-GFP+(*green*) and immunostained CD3+ T (*red*) cells of ventricular origin in the peri-infarct cortex (marked by a *cross*). The nucleus is stained with DAPI (*blue*). *Scale bar* 10 μm. **c** Quantification of three independent animals per time point for PA-GFP-negative (*red*) and PA-GFP-positive (*green*) T cells, 4 days after pMCAo and indicated time points after illumination per one coronal section at the bregma level in the ipsilateral hemisphere. **d** Corresponding accumulative topographic maps of PA-GFP+CD3+ photoactivated T cells at the indicated time points after stroke from three individual animals. **e** Experimental design for estimating cerebral T-cell counts entering via the ChP over a 24 h time period at the peak infiltration period after stroke (d4–d5). **f** Schematic illustration of the optogenetic setup for intraventricular photoactivation of PA-GFP T cells. **g** Quantification of PA-GFP-negative (*red*) and PA-GFP-positive (*green*) T cells, 4 days after pMCAo without illumination ($n = 10$) or with 24 h of constant illumination ($n = 7$) per one coronal section at the bregma level in the ipsilateral hemisphere and **h** calculation of the percentage of ventricularly photoconverted PA-GFP+ and PA-GFP−CD3+ T cells in the ipsilateral hemisphere after subtraction of baseline T-cell counts before 24-h illumination at 4 days after pMCAo. All comparative analyses are illustrated as mean ± SD

intraparenchymal migration from the lateral ventricle to the cortex along the corpus callosum.

Notably, a single 5 min pulse for PA-GFP activation in the lateral ventricle resulted in optical labeling of more than 50% of T cells detected in the peri-infarct cortex analyzed at the late time points after photoactivation (8 and 12 h, Fig. 2c, d). Yet, this experiment was not able to precisely estimate the proportion of cerebral T cells entering via the ChP. Therefore, we performed a similar intraventricular photoactivation experiment starting 4 days after stroke induction, however, with prolonged illumination over 24 h of freely behaving mice using an optogenetic illumination setup and killing the animals directly at the end of the illumination period in awake, freely moving mice (Fig. 2e, f). We aimed to determine a rough estimate for the ratio of invading T cells via the ipsilateral ChP in the lateral ventricle or by other invasion routes over this 24-h period from 4 to 5 days after stroke by subtracting the number of T cells detected at 4 days post-lesion (i.e., before intraventricular photoactivation, Fig. 2g), which was determined in a second set of control-operated animals without intraventricular illumination. Importantly, long-term photoactivation of the lateral ventricle itself did not induce an inflammatory reaction compared to mice that underwent the same procedure without illumination (Suppl. Figure 4). Hereby, we detected by this approximation that about two-thirds of the T cells infiltrated via the ChP of the ipsilateral ventricle while one-third of T cells infiltrated along other pathways (Fig. 2g, h), confirming that the ChP of the lateral ventricle is the predominant invasion route for T cells after cortical infarction.

Choroidal T cells invade the brain parenchyma

The above-shown results obtained in the UBC-PA-GFP mouse model suggested infiltration of T cells through the ChP and migration to the peri-infarct cortex along the corpus callosum. Surprisingly, the neuroanatomical structure of the ChP of lateral ventricles in adult mice as well as the exact migration pathway of T cells from the ChP stroma to the brain parenchyma have previously not been well described. Therefore, we performed light-sheet microscopy of lectin-perfused and cleared brains enabling 3-dimensional visualization of choroidal vascularization and its anatomical junction to the ventricle wall. In accordance with previous studies on ChP development during embryogenesis [23], we detected attachment of the ChP to the medial wall of the lateral ventricle (Fig. 3a, b) clearly visible by vasculature penetrating from the brain parenchyma into the ChP (Suppl. video). 3-dimensional reconstruction of segmented ChP, lateral ventricle and the corpus callosum revealed the close proximity of these anatomical structures (Fig. 3c, d). Therefore, we hypothesized that T cells shall be able to directly invade the brain parenchyma from the ChP stroma, avoiding first the entry into the CSF via the tight BCSFB and passage through the CSF. This hypothesis was further supported by detecting eGFP-positive T cells localized along the proposed invasion route from the ChP stroma, the medio-basal ventricle wall, the apical corpus callosum (CC) and along the CC to the peri-ischemic infarct in lymphocyte-deficient $Rag1^{-/-}$ mice reconstituted with eGFP + T cells (Fig. 3e, f). Finally, to test the potential alternative migration route of T cells from the ChP to the cortex via the CSF, we blocked this migration pathway by matrigel injection into the ipsilateral ventricle (Fig. 3f). Matrigel—a non-toxic agent polymerizing at body temperature—was confined to the ipsilateral ventricle and did not diffuse to lower compartments (Fig. 3g). Moreover, this technique of blocking CSF flow and intraventricular leukocyte migration was previously shown to not induce neuroinflammation or affect ChP integrity [36]. Blocking of CSF flow by matrigel injection did not significantly alter T-cell counts at the peri-ischemic infiltration site compared to control-operated mice (needle introduction and PBS injection), indicating that intraventricular lymphocytes as well as migration via the ventricular CSF space might not play a significant role for cerebral T-cell invasion after stroke (Fig. 3h).

Choroid plexus infarction reduces post-stroke T-cell invasion

Several previous reports demonstrated that experimental brain ischemia by transient, proximal occlusion of the
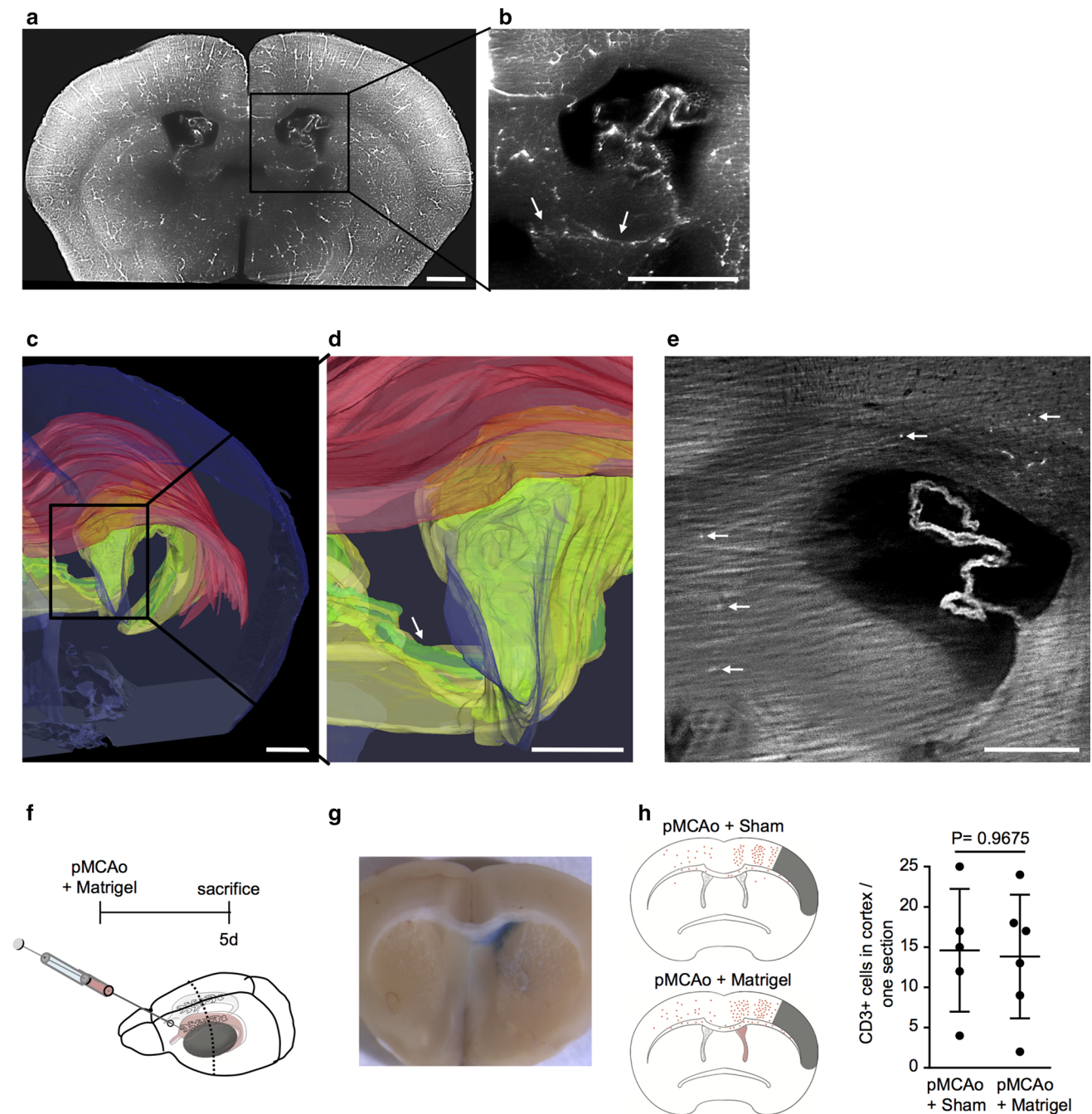
Fig. 3 Choroidal T cells directly invade the brain parenchyma. **a, b** Coronal image from a lectin-perfused, cleared brain. *Arrows* highlight penetrating cerebral vessels to the ChP, indicating the ChP–brain parenchyma junction. *Scale bar* 0.5 mm. **c–d** Lectin-perfused solvent-cleared brains have been imaged by light-sheet microscopy and segmented for brain parenchyma (*blue*), the ChP (*green*), ventricle (*yellow*) and the corpus callosum (*red*) in order to illustrate the anatomical relation of these structures presumably involved in intraparenchymal T-cell migration. Arrows indicate the junction of the ChP stroma with the brain parenchyma at the mediobasal ventricle wall. *Scale bar* 0.5 mm. **e** Source image used for the 3D reconstruction shown in Fig. 1c. *Arrows* indicate eGFP + T cells which have been transferred to lymphocyte-deficient $Rag1^{-/-}$ mice for T-cell-specific identification in solvent-cleared brains, *scale bar* 250 μm. **f** Experimental design to block intraventricular cell migration by injection of matrigel into the ipsilateral ventricle. **g** Representative image illustrating polymerized matrigel inside the left lateral ventricle. Matrigel was supplemented with *Evans blue* for a better visualization of the matrigel in this image. **h** Accumulative topographic maps and **i** quantification of CD3$^+$ T cells per one ipsilateral coronal brain section at bregma location 5 days after pMCAo + Sham or pMCAo + matrigel treatment ($n = 6$ per group, three independent experiments). Comparative analyses are represented as mean ± SD

MCA (tMCAo model) resulted in substantially lower T-cell infiltration despite much larger infarcts than after permanent, distal occlusion of the MCA (pMCAo model) [20, 47]. Following the previous results revealing the ChP as a key invasion route for cerebral T-cell invasion after stroke, we tested the hypothesis that proximal MCA occlusion might affect ChP function thereby resulting in reduced T-cell invasion. Hence, we analyzed T-cell infiltration 3 days after pMCAo or tMCAo (Fig. 4a). In accordance with our previous studies, large ischemic lesions in the tMCAo model resulted in significantly lower T-cell infiltration compared to cortical lesions in the pMCAo model (Fig. 4b). Impaired post-ischemic T-cell infiltration in the tMCAo model was associated with a more than twofold increase in TUNEL+ cells of the ipsilateral ChP stroma, while distal MCA occlusion in the pMCAo model did not induce choroidal cell death compared to the contralateral control ChP (Fig. 4c, d). Ischemic lesion after proximal occlusion of the MCA is fully compatible with the transient occlusion of the anterior

choroidal artery, which supplies predominantly the ChP and originates from the proximal MCA [3, 11]. To further corroborate the critical role of the ChP in post-stroke T-cell invasion, we induced a localized photothrombotic (PT) lesion of the ipsilateral ChP directly after pMCAo by a laser probe introduced into the ipsilateral ventricle (Fig. 4e, f). 5 days after surgery, cell death was observed specifically in the ChP after PT (Fig. 4f) and we detected a significant reduction in total cerebral T-cell counts in mice undergoing choroidal photothrombosis (pMCAo + PT) in comparison to sham-operated (pMCAo + Sham) mice (Fig. 4g, h). More specifically, choroidal infarction massively reduced cortical T-cell invasion while some T cells were detected in the caudal ventricle region most likely as a reaction to the photothrombotic lesion itself (Fig. 4f, g). Notably, we did not detect a significantly difference in the infarct volume in mice with choroidal photothrombosis (pMCAo + PT) in comparison to sham-operated animals (pMCAo + Sham) (Fig. 4i) despite the substantial reduction in T-cell infiltration. These
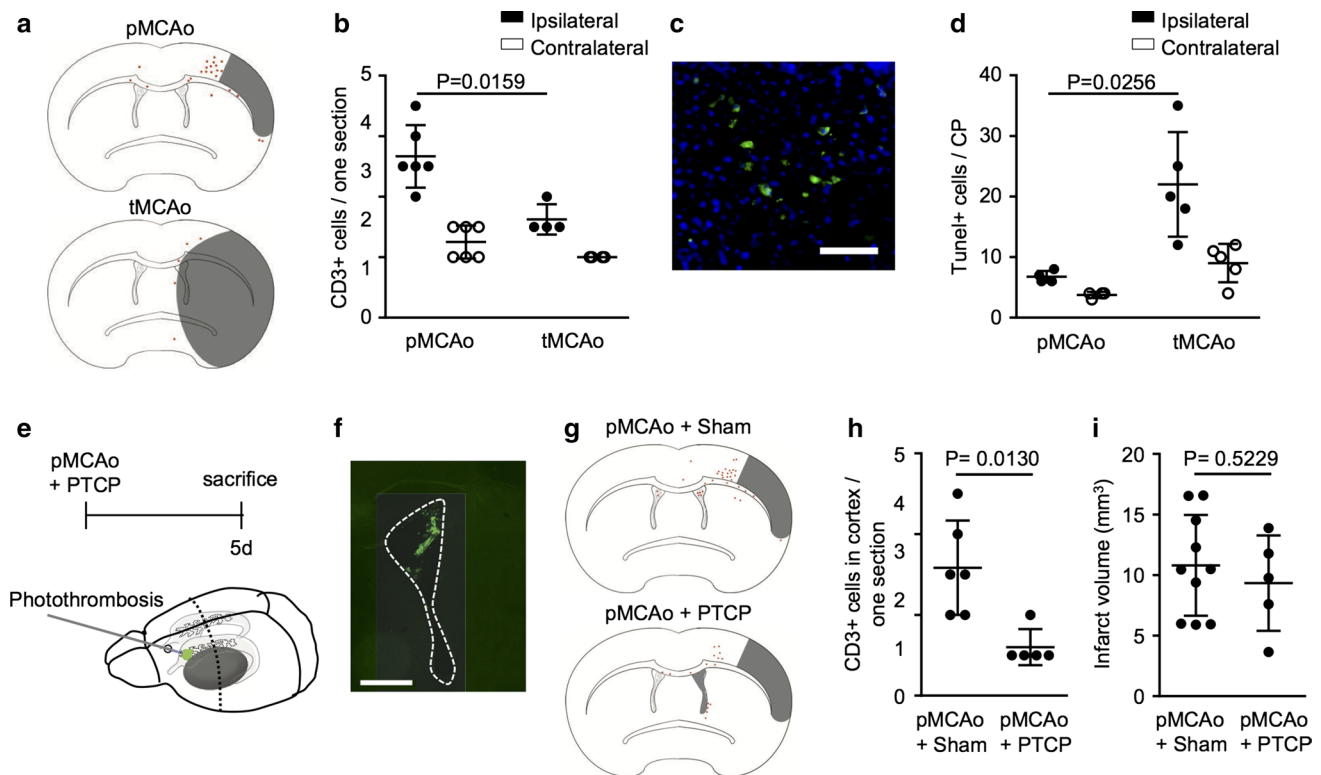

Fig. 4 Choroid plexus infarction reduces T-cell invasion after cortical ischemia. **a** Cumulative topographic maps of one coronal section from six mice (*each dot* represents one cell, infarct area shown in *gray*) and **b** quantitative analysis of T cells per one ipsilateral and contralateral hemisphere section at bregma level 3 days after pMCAo or tMCAo (*n* = 6 per group). **c** Representative image of TUNEL+ (*green*) stained apoptotic cells within the ChP of the ipsilateral ventricle 24 h after tMCAo; nuclear stain with DAPI (*blue*). *Scale bar* 50 μm. **d** Quantitative analysis of TUNEL-positive cells per one ipsilateral and contralateral ChP 24 h after pMCAo or tMCAo (*n* = 4–5).

e Experimental design to test the role of the ChP in post-stroke T-cell infiltration by an isolated photothrombotic ChP lesion (PT-ChP). **f** Representative image of TUNEL+ (*green*) stained apoptotic cells within the ChP of the ipsilateral ventricle 5 days after pMCAo + PT-ChP. *Scale bar* 500 μm. **g** Cumulative topographic maps of T cells from one section at bregma level from five mice per group, 5 days after pMCAo + Sham or pMCAo + PT-ChP surgery. **h** Quantification of cortical T cells in both groups per one coronal section in the ipsilateral hemisphere and **i** infarct volume of both treatment groups (*n* = 5 per group)
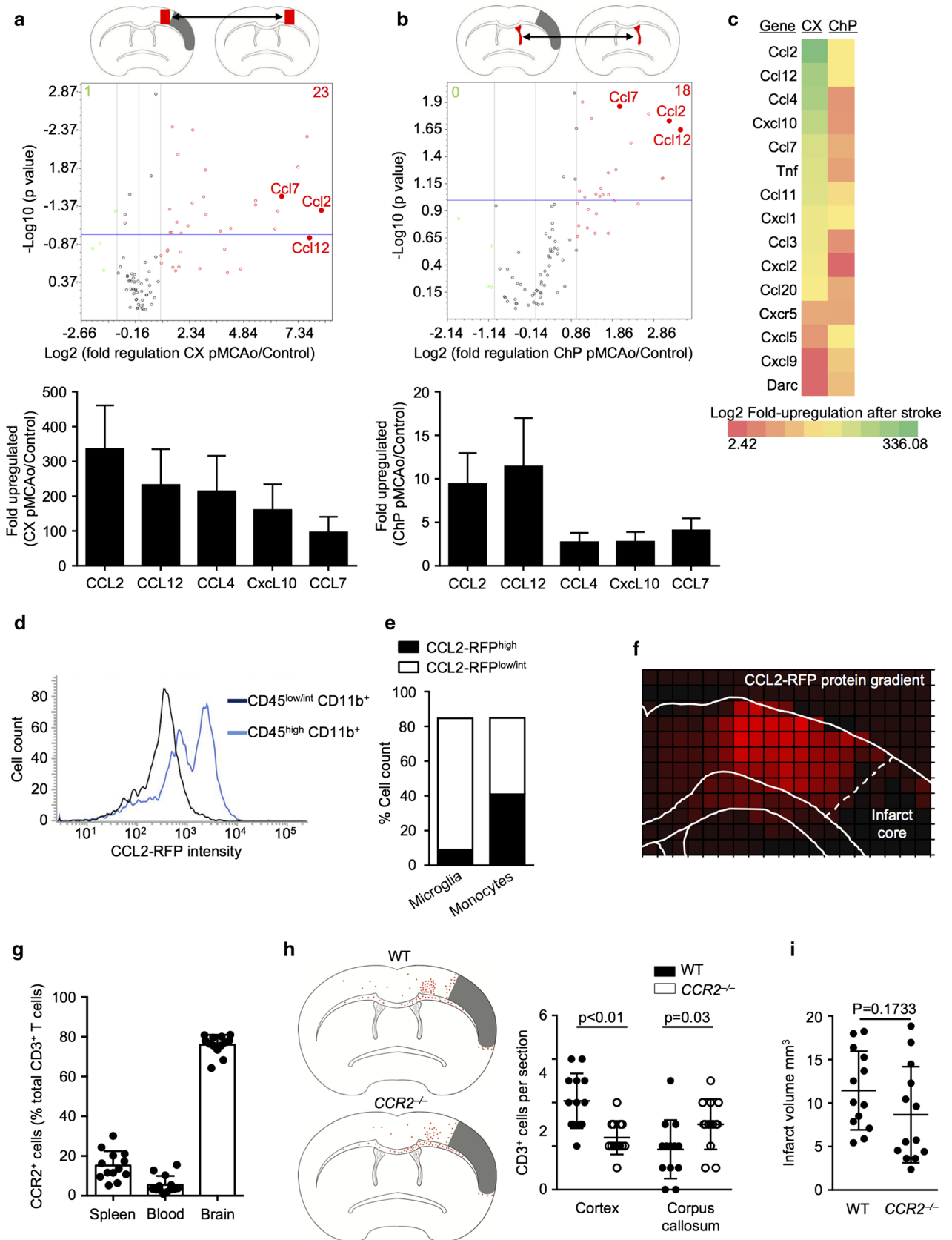
◄**Fig. 5** Intraparenchymal T-cell migration follows a CCR2-ligands gradient between peri-infarct cortex and choroid plexus. **a**, **b** Volcano plot illustration of the regulation of gene expression of 84 chemokines and chemokine receptors (*upper panels*) and bar graphs for top 5 regulated genes (*lower panels*) in **a** the cortex (CX) and **b** the ChP between 24 h after pMCAo or Sham surgery (*n* = 6 per group, 3 individual experiments per analysis). **c** Heat map of the top 10 upregulated genes in the cortex and ChP24h after pMCAo compared to Sham surgery, indicating substantial differences in the magnitude of regulation of the same genes in the CX and ChP after pMCAo. **d** Representative histogram of the expression intensity of CCL2-RFP in the CD45$^{low/int}$CD11b$^+$microglial population and CD45^{high}CD11b$^+$ monocytes 24 h after pMCAo. **e** Quantification of "high" and "low/intermediate" CCL2-RFP expression cells within the microglial and monocyte cell populations corresponding to the cell populations shown in panel D. **f** Illustration of rasterized, relative CCL2-RFP expression intensity normalized to the homotypic contralateral hemisphere (see "Materials and methods" section for details) 24 h after pMCAo in the ipsilateral hemisphere revealing a CCL2 focus in the peri-infarct cortex. *Dashed line* indicates the border to the infarct core. **g** Frequency of CCR2-positive cells among total T cells (CD3) was analyzed by flow cytometry 5 days after stroke in spleen, blood and the ipsilateral brain hemisphere. **h** Cumulative topographic maps (*left*; 13 mice per group) and quantification (*right*) of T-cell counts 5 days after pMCAo in WT and CCR2$^{-/-}$mice per one coronal section in ipsilateral cortex and corpus callosum and **i** infarct volume of both groups (*n* = 13 per group, 2 individual experiments)

results clearly demonstrate the importance of the ChP for post-stroke T-cell infiltration, however, without affecting stroke severity in contrast to previous studies linking cerebral T-cell infiltration to stroke outcome.

CCL2 chemokine gradient between the peri-infarcted cortex and choroid plexus

We next aimed at investigating the molecular basis for the directed intracerebral migration of T cells from the ChP to the peri-infarct cortex and hypothesized an underlying chemokine gradient between cortex and the ChP to be responsible for this fast intraparenchymal T-cell migration. Therefore, we performed a PCR array for 84 chemokines and chemokine receptors from microdissected samples of ChP and the peri-infarct cortex 24 h after pMCAO and control animals. We detected 23 up-regulated genes in the peri-infarct compared to control cortex (Fig. 5a; Suppl. Table 4) and 18 up-regulated genes in the post-stroke ChP compared to control ChP (Fig. 5b; Suppl. Table 5), using twofold regulation and *p* < 0.1 as significant thresholds. Interestingly, the two most abundantly upregulated chemokines in the cortex after stroke—CCL2 and CCL12—were also most highly upregulated in the post-ischemic ChP. However, overall chemokine upregulation was manifold higher in the peri-infarct cortex compared to the ipsilateral ChP with, e.g., more than 300-fold upregulation of CCL2 in the cortex compared to a tenfold upregulation in the ChP after stroke (Fig. 5a–c), suggesting a biologically relevant gradient for

these chemokines between cortex and ChP. Notably, three out of the five most abundantly upregulated chemokines in the cortex as well as in the ChP are ligands of the CC chemokine receptor 2 (CCR2), namely CCL2, CCL12 and CCL7 [17, 19, 27]. This indicated a potentially relevant involvement of the CCR2 chemokine axis in post-ischemic T-cell attraction from the ChP to the peri-infarct cortex. To reveal the cellular source of cortical CCL2 expression after stroke, we performed a flow cytometric analysis of *CCL2-RFP* reporter mice 24 h after stroke induction. Here, we detected CD45$^{low/int}$CD11b$^+$ (presumably microglia) and CD45^{high}CD11b$^+$ (presumably monocyte/macrophages) as the main RFP positive cells, however, with differences in CCL2-RFP expression levels between these two populations (Fig. 5d). While microglial cells displayed homogenous low-intermediate CCL2-RFP expression levels, we detected two distinct subpopulations of CD45^{high}monocytic cells with low/intermediate and high CCL2-RFP expression, respectively (Fig. 5d, e). Next, we analyzed histologically coronal brain sections of *CCL2-RFP* reporter mice to test for the cellular source of the regional chemokine gradient suggested by the results of the PCR array. Indeed, after rasterizing the fluorescence intensity images and generating density maps, we detected a marked gradient of RFP expression with its center at the same anatomical area of predominant T-cell invasion in the peri-infarct cortex (Fig. 5f). Notably, this CCL2 gradient focusing in the peri-infarct cortex was observed already at early time points after stroke (24 h post-lesion) preceding cerebral T-cell invasion and can, therefore, be assumed rather as a cause than a consequence of cortical T-cell clustering. Taken together, our chemokine screening analysis identified CCR2 ligands being substantially upregulated after stroke and we were able to confirm a relevant CCL2 gradient also at the protein level, mainly secreted by innate immune cells in the peri-infarct cortex. Consequently, we hypothesized that CCR2 might be involved in attraction of T cells from the ChP along the CCL2 gradient to the peri-infarct cortex. Analyzing the organ-specific frequency of CCR2$^+$ T cells in the peripheral immune compartment (spleen, blood) and the post-ischemic brain, we observed a substantial enrichment of CCR2$^+$ T cells in the ischemic hemisphere supporting a potential role of CCR2 in cerebral T cells migration (Fig. 5g). We next aimed to block the CCR2 chemokine axis using *CCR2$^{-/-}$* mice to probe its impact on post-stroke T-cell migration. CCR2-deficiency indeed significantly reduced T-cell migration to the peri-infarct cortex. Interestingly, lack of CCR2 resulted in slightly increased T-cell counts in the corpus callosum (Fig. 5h). Notably, we did not detect a significant difference in infarct volume between groups, indicating a stroke severity-independent effect of CCR2 expression in T-cell migration (Fig. 5i). This finding suggests that chemotaxis driven by CCR2 ligands might be important for intracerebral

migration along a chemokine gradient to the peri-infarct region but might not be involved for initial entry of T cells through the ChP.

The role of choroid plexus after stroke in humans

Next, we aimed to test the involvement of the ChP for post-stroke cerebral T-cell invasion in human stroke patients. For this, we obtained autopsy samples of both lateral ventricles from five stroke patients dying of other cause than stroke in the subacute phase after stroke onset and six control patients without cerebral infarction (Suppl. Table 2). By histological analysis for T cells (CD3) and monocytes/

macrophages (CD68) (Fig. 6a), we observed increased choroidal T-cell counts in stroke patients compared to control patients (Fig. 6b). Moreover, in accordance with the results obtained in the mouse stroke models, T cells were the main cell population in the ChP of stroke patients (Fig. 6b). We then analyzed the chemokine expression in human samples of the peri-infarct cortex and the contralateral homotypic control cortex from autopsy samples of six patients, which had died in the acute phase after stroke (Suppl. Table 3). We performed a NanoString analysis for quantitative transcriptional regulation of 561 inflammation-related human genes, revealing a distinct upregulation of 8 inflammatory genes in the peri-infarct cortex compared to the contralateral side
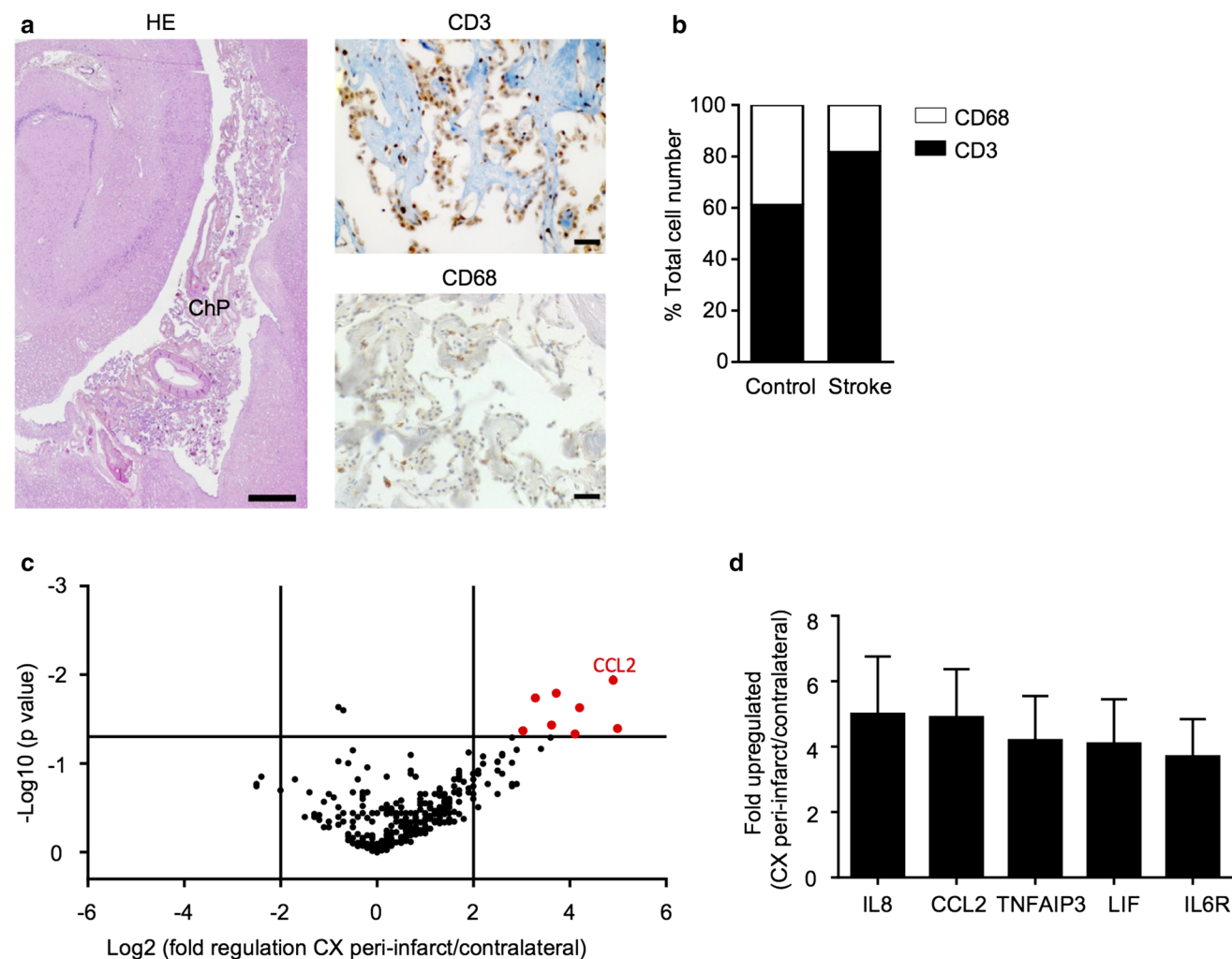
Fig. 6 Choroid plexus cellularity and cortical chemokines in human stroke patients. **a** Representative images of a hematoxylin–eosin-stained section of the human choroid plexus in the temporal horn of the lateral ventricle and surrounding brain tissue (*left, scale bar* 1 mm), CD3+ T cell and CD68+ monocytes/macrophage stainings (CD68) (*right, scale bars* 40 μm) used for subsequent analysis. **b** Quantitative analysis of the ratio between CD68 and CD3 positive cells in the ipsilateral ChP of control patients or stroke patients

($n = 5–6$ per group, see Suppl. Table 2). **c** Volcano plot depicting the regulation of gene expression assessed by Nanostring analysis between the ipsilateral peri-infarct tissue and homotypic contralateral side in patients in the acute phase after ischemic stroke (see Suppl. Table 3). *Red dots* indicate the significantly upregulated genes in the peri-infarct tissue. **d** Bar graph showing fold regulation of the top 5 significantly upregulated genes in the peri-infarct cortex compared to the contralateral hemisphere ($n = 6$ per group)

(Fig. 6c). Also in these human samples, CCL2 was one of the overall most highly upregulated genes, and together with IL-8 (CXCL8) the only significantly upregulated chemokine (Fig. 6d; Suppl. Table 6). These results demonstrate a remarkable similarity for the cellular infiltration pattern as well as cortical chemokine expression after human stroke compared to the murine stroke model, suggesting that a comparable intraparenchymal T-cell migration from the ChP to the ischemic lesion might also occur after human stroke.

Discussion

We describe in this study the ChP as a previously unrecognized critical invasion route for T cells into the ischemic brain after stroke. This finding of choroidal T-cell infiltration after stroke offers an explanation of previously elusive observations in the field of stroke immunology such as the specific clustering of T cells in the peri-infarct cortex, differences in T-cell invasion between stroke models and finally the ineffectiveness of blocking post-stroke T-cell invasion by targeting endothelial adhesion molecules in several previous reports.

Lymphocyte infiltration after stroke has become a main research area in experimental stroke research due to the implication of post-stroke neuroinflammation in secondary brain damage [4, 44]. However, preclinical research on post-stroke neuroinflammation has repetitively experienced irreproducibility of findings between laboratories using different stroke models and reported substantial differences in the extent of neuroinflammation between commonly used mouse models of acute brain ischemia [8, 47]. While models of permanent ischemia in the cerebral cortex (pMCAo, photothrombosis, thrombin-injection model) have reproducibly resulted in a pronounced cellular neuroinflammation, more extensive lesions induced by transient occlusion of the proximal MCA resulted in less cerebral leukocyte infiltration [6, 20, 47]. In the present study, we observed that only transient, proximal MCA occlusion induced cell death in the ipsilateral ChP, most likely by occlusion of the supplying anterior choroidal artery. Taking into account that based on our results approximately 60% of cerebral T cells invade via the ipsilateral ChP, it seems plausible that differential ChP damage in some stroke models accounts for a large part of inter-laboratory and -model differences observed in previous studies on post-stroke neuroinflammation.

In contrast to the endothelium of the BBB, the ChP endothelium is fenestrated, facilitating cellular migration into the ChP stroma. On the other side, the tight junctions of the ChP epithelium contribute to the BCSFB by limiting paracellular transport of small molecules and immune cell entry into the CSF [29, 35, 38]. These anatomical properties of the ChP implicate that circulating leukocytes can

easily enter the ChP stroma but crossing the epithelial layer into the CSF would be far more energy demanding. Previous studies have proposed that ChP-resident T cells can be readily mobilized for cerebral invasion under inflammatory conditions. T cells in the ChP have in principle two routes to invade the brain parenchyma: crossing the epithelial layer into the CSF and invading the brain from the CSF at different sites or migrate from the ChP stroma directly into the brain parenchyma at the base of the ChP. The involvement of both invasion pathways for T cells from the ChP stroma have been barely investigated under physiological conditions or inflammatory brain disorders; nevertheless, the migration pathway via the CSF has been assumed in the majority of studies analyzing the ChP in autoimmune brain diseases [13, 33]. Yet, the migration of lymphocytes across the BCSFB remained questionable as the key adhesion molecules involved in this process—ICAM-1 and VCAM-1—are exclusively expressed on the apical side of ChP epithelial cells, thus, not accessible for stromal lymphocytes to enter the CSF [37, 46]. This means that key adhesion molecules which are expressed and critical for cell trafficking at the BBB are also expressed in the ChP but are not functional for T-cell invasion to the ChP because these molecules are not accessible for circulating leukocytes. This is of high clinical relevance, as the specific inhibition of endothelial or leukocyte adhesion molecules involved at the BBB failed so far to improve clinical outcome in stroke patients [12, 16] in contrast to numerous preclinical studies showing improved stroke outcome by depleting or reducing circulating lymphocytes. These discrepant findings might be attributable to the wrong assumption that cerebral T-cell invasion occurs along the vascular invasion routes, thereby targeting vascular adhesion molecules that play only a minor role at the ChP.

The results from our study unexpectedly suggest a rapid and directed T-cell migration from the ChP to the brain parenchyma. We have demonstrated the previously insufficiently investigated attachment of the ChP in the mouse lateral ventricle at the basomedial ventricle wall as a possible entry site for T cells into the CNS. Border structures such as tanycytes surrounding circumventricular organs or other cell types with tight intercellular junctions have to our knowledge not been described at the ChP base. The junction of the ChP to the brain parenchyma remains, therefore, a matter of debate and further neuroanatomical studies are urgently needed to clarify the anatomical basis for direct cell entry from the ChP stroma to the brain parenchyma. Here, we identified T cells after photoactivation in the ChP along the ChP–parenchyma junction, the corpus callosum and the peri-infarct cortex. Moreover, inhibition of CSF circulation did not affect cerebral T-cell invasion, strongly supporting a not yet considered migration from the ChP stroma into the brain parenchyma. Additional indirect indication for this novel migration pathway was the surprisingly

fast kinetics of T-cell translocation from the ventricle/ChP after photoactivation to the peri-infarct cortex within only few hours, which seems neither compatible with the passive transport of ventricular T cells along CSF flow nor the highly energy-demanding and tightly regulated migration across the BCSFB into the lateral ventricle and then across the ventricular ependymal cell layer directly into the forebrain parenchyma.

Results from our experiments in *CCR2*$^{-/-}$ mice support the concept of CCR2-dependent intraparenchymal migration of T cells after the parenchymal invasion from the ChP stroma. While potential mechanisms in ChP activation and recruitment of inflammatory cells into the ChP have previously been studied—and Type I Interferons been defined as key mediators—molecular cues for intraparenchymal T-cell migration have to our knowledge previously not been characterized. We have observed a distinct gradient for CCR2 ligands (i.e., CCL2, CCL7, CCL12) between the peri-infarct cortex and the ipsilateral ChP and have additionally defined innate immune cells in the peri-infarct cortex as their main source. However, we cannot exclude that the observed effects in the *CCR2*$^{-/-}$ model might be at least partially due to a generally ameliorated inflammatory milieu in the ischemic brain as we used in these experiments a global *CCR2*-knockout model. Particularly, studies in models of primary autoimmune neuroinflammation have shown a key role of CCR2 in recruiting monocytes and dendritic cells to the inflamed brain [7]. On the other side, a study by Chu et al. using a permanent MCA occlusion model as in our study revealed CCR2-independent recruitment of inflammatory monocytes to the ischemic brain [5] and resident microglial cells are sufficient to produce large amounts of T-cell-attractive CCL2 in response to brain injury [15, 40].

Based on the results from our study showing a predominant T-cell infiltration via the ChP route, it is conceivable that previous preclinical studies as well as current clinical trials testing specific blockage of T-cell migration across the BBB after acute brain ischemia might have been hampered by the alternative choroidal invasion route. Finally, further alternative invasion routes such as the meningeal entry site need to be further investigated [2]. Additional studies characterizing the distinct adhesion molecules involved at migration across the different brain barriers of the BBB, the BCSFB or alternative invasion sites such as the meninges are inevitable for the rationale design of clinical stroke trials targeting at cerebral T-cell invasion. Notably, results from previous studies analyzing both invasion routes into the brain under conditions of primary autoimmune neuroinflammation might be of only limited value due to the specific properties of stroke-induced inflammation such as the acute onset, pronounced glial activation and additional peripheral immunomodulation. Besides the complexity of

various potential invasion routes of inflammatory leukocytes after acute brain, evasion pathways for lymphocytes from the post-ischemic brain to exit the brain and potentially re-enter the blood stream are unknown. Various routes have previously been described for lymphocytes to exit the brain parenchyma under inflammatory conditions including a recently described cerebral lymphatic system [22]. However, the contribution of potential evasion mechanisms for cerebral lymphocyte turnover rates after stroke is unknown. Therefore, the model in this study revealing rapid translocation from the ChP to the peri-infarct cortex in UBC-PA-GFP mice is limited by the assumption of a static system with no substantial T-cell turnover within 24 h after cell invasion.

Taken together, we observed an unexpected role of the ipsilateral ChP in the lateral ventricle as the major invasion route for T cells into the ischemic brain after stroke. We have defined the intracerebral migration route from the ChP into the peri-infarct cortex via a ChP–parenchyma junction, detected a potential chemokine gradient involved in the intraparenchymal migration and confirmed similar mechanisms in the human brain after acute stroke. These results question previously accepted concepts and therapeutic strategies in post-stroke neuroinflammation and are of direct clinical relevance for current and planned clinical trials testing therapies for inhibiting post-stroke cerebral leukocyte invasion.

Author contributions G.L., C.B., X.M., G.E., R.C., T.A., I.L., S.L., and L.M. performed experiments; G.L., C.B., A.G., T.A., R.M., A.E., N.P., B.E. and A.L. analyzed data; J.M. provided critical material and analyzed data; D.V., C.H., N.P., B.E. and G.L. contributed critical input to the manuscript; A.L. initiated the study, designed experiments and wrote the manuscript.

References

1. Becker K, Kindrick D, Relton J, Harlan J, Winn R (2001) Antibody to the alpha4 integrin decreases infarct size in transient focal cerebral ischemia in rats. Stroke 32:206–211

2. Benakis C, Brea D, Caballero S, Faraco G, Moore J, Murphy M, Sita G, Racchumi G, Ling L, Pamer EG et al (2016) Commensal microbiota affects ischemic stroke outcome by regulating intestinal gammadelta T cells. Nat Med 22:516–523. doi:10.1038/nm.4068

3. Canazza A, Minati L, Boffano C, Parati E, Binks S (2014) Experimental models of brain ischemia: a review of techniques, magnetic resonance imaging, and investigational cell-based therapies. Front Neurol 5:19. doi:10.3389/fneur.2014.00019

4. Chamorro A, Meisel A, Planas AM, Urra X, van de Beek D, Veltkamp R (2012) The immunology of acute stroke. Nat Rev Neurol 8:401–410. doi:10.1038/nrneurol.2012.98

5. Chu HX, Kim HA, Lee S, Broughton BR, Drummond GR, Sobey CG (2016) Evidence of CCR2-independent transmigration of Ly6C(hi) monocytes into the brain after permanent cerebral ischemia in mice. Brain Res 1637:118–127. doi:10.1016/j.brainres.2016.02.030

6. Chu HX, Kim HA, Lee S, Moore JP, Chan CT, Vinh A, Gelderblom M, Arumugam TV, Broughton BR, Drummond GR et al (2014) Immune cell infiltration in malignant middle cerebral artery infarction: comparison with transient cerebral ischemia. J Cereb Blood Flow Metab Off J Int Soc Cereb Blood Flow Metab 34:450–459. doi:10.1038/jcbfm.2013.217

7. Clarkson BD, Walker A, Harris MG, Rayasam A, Sandor M, Fabry Z (2015) CCR2-dependent dendritic cell accumulation in the central nervous system during early effector experimental autoimmune encephalomyelitis is essential for effector T cell restimulation in situ and disease progression. J Immunol 194:531–541. doi:10.4049/jimmunol.1401320

8. Dirnagl U (2006) Bench to bedside: the quest for quality in experimental stroke research. J Cereb Blood Flow Metab 26:1465–1478. doi:10.1038/sj.jcbfm.9600298

9. Dirnagl U (2014) Modeling immunity and inflammation in stroke: can mice be trusted? Stroke J Cereb Circ 45:e177–e178. doi:10.1161/STROKEAHA.114.005640

10. Donnan GA, Fisher M, Macleod M, Davis SM (2008) Stroke. Lancet 371:1612–1623. doi:10.1016/S0140-6736(08)60694-7

11. Dorr A, Sled JG, Kabani N (2007) Three-dimensional cerebral vasculature of the CBA mouse brain: a magnetic resonance imaging and micro computed tomography study. NeuroImage 35:1409–1423. doi:10.1016/j.neuroimage.2006.12.040

12. Elkins J (2016) Primary results of the ACTION trial of natalizumab in acute ischemic stroke (AIS). International stroke conference

13. Engelhardt B, Ransohoff RM (2012) Capture, crawl, cross: the T cell code to breach the blood-brain barriers. Trends Immunol 33:579–589. doi:10.1016/j.it.2012.07.004

14. Iadecola C, Anrather J (2011) The immunology of stroke: from mechanisms to translation. Nat Med 17:796–808. doi:10.1038/nm.2399

15. Inose Y, Kato Y, Kitagawa K, Uchiyama S, Shibata N (2015) Activated microglia in ischemic stroke penumbra upregulate MCP-1 and CCR2 expression in response to lysophosphatidylcholine derived from adjacent neurons and astrocytes. Neuropathology 35:209–223. doi:10.1111/neup.12182

16. Investigators EAST (2001) Use of anti-ICAM-1 therapy in ischemic stroke: results of the Enlimomab Acute Stroke Trial. Neurology 57:1428–1434

17. Kuscher K, Danelon G, Paoletti S, Stefano L, Schiraldi M, Petkovic V, Locati M, Gerber BO, Uguccioni M (2009) Synergy-inducing chemokines enhance CCR2 ligand activities on monocytes. Eur J Immunol 39:1118–1128. doi:10.1002/eji.200838906

18. Liesz A, Zhou W, Mracsko E, Karcher S, Bauer H, Schwarting S, Sun L, Bruder D, Stegemann S, Cerwenka A et al (2011) Inhibition of lymphocyte trafficking shields the brain against deleterious neuroinflammation after stroke. Brain J Neurol 134:704–720. doi:10.1093/brain/awr008

19. Lim JK, Obara CJ, Rivollier A, Pletnev AG, Kelsall BL, Murphy PM (2011) Chemokine receptor Ccr2 is critical for monocyte accumulation and survival in West Nile virus encephalitis. J Immunol 186:471–478. doi:10.4049/jimmunol.1003003

20. Llovera G, Hofmann K, Roth S, Salas-Perdomo A, Ferrer-Ferrer M, Perego C, Zanier ER, Mamrak U, Rex A, Party H et al (2015) Results of a preclinical randomized controlled multicenter trial (pRCT): anti-CD49d treatment for acute brain ischemia. Sci Transl Med 7:299ra121. doi:10.1126/scitranslmed.aaa9853

21. Llovera G, Roth S, Plesnila N, Veltkamp R, Liesz A (2014) Modeling stroke in mice: permanent coagulation of the distal middle cerebral artery. J Vis Exp JoVE:e51729. doi:10.3791/51729

22. Louveau A, Harris TH, Kipnis J (2015) Revisiting the mechanisms of CNS immune privilege. Trends Immunol 36:569–577. doi:10.1016/j.it.2015.08.006

23. Lun MP, Monuki ES, Lehtinen MK (2015) Development and functions of the choroid plexus-cerebrospinal fluid system. Nat Rev Neurosci 16:445–457. doi:10.1038/nrn3921

24. Macrez R, Ali C, Toutirais O, Le Mauff B, Defer G, Dirnagl U, Vivien D (2011) Stroke and the immune system: from pathophysiology to new therapeutic strategies. Lancet Neurol 10:471–480. doi:10.1016/S1474-4422(11)70066-7

25. Moskowitz MA, Lo EH, Iadecola C (2010) The science of stroke: mechanisms in search of treatments. Neuron 67:181–198. doi:10.1016/j.neuron.2010.07.002

26. Neumann J, Riek-Burchardt M, Herz J, Doeppner TR, Konig R, Hutten H, Etemire E, Mann L, Klingberg A, Fischer T et al (2015) Very-late-antigen-4 (VLA-4)-mediated brain invasion by neutrophils leads to interactions with microglia, increased ischemic injury and impaired behavior in experimental stroke. Acta Neuropathol 129:259–277. doi:10.1007/s00401-014-1355-2

27. Nibbs RJ, Graham GJ (2013) Immune regulation by atypical chemokine receptors. Nat Rev Immunol 13:815–829

28. Pan C, Cai R, Quacquarelli FP, Ghasemigharagoz A, Lourbopoulos A, Matryba P, Plesnila N, Dichgans M, Hellal F, Erturk A (2016) Shrinkage-mediated imaging of entire organs and organisms using uDISCO. Nat Methods 13:859–867. doi:10.1038/nmeth.3964

29. Ransohoff RM, Engelhardt B (2012) The anatomical and cellular basis of immune surveillance in the central nervous system. Nat Rev Immunol 12:623–635. doi:10.1038/nri3265

30. Ransohoff RM, Kivisakk P, Kidd G (2003) Three or more routes for leukocyte migration into the central nervous system. Nat Rev Immunol 3:569–581. doi:10.1038/nri1130

31. Relton JK, Sloan KE, Frew EM, Whalley ET, Adams SP, Lobb RR (2001) Inhibition of alpha4 integrin protects against transient focal cerebral ischemia in normotensive and hypertensive rats. Stroke 32:199–205

32. Saederup N, Cardona AE, Croft K, Mizutani M, Cotleur AC, Tsou CL, Ransohoff RM, Charo IF (2010) Selective chemokine receptor usage by central nervous system myeloid cells in CCR2-red fluorescent protein knock-in mice. PLoS One 5:e13693. doi:10.1371/journal.pone.0013693

33. Schwartz M, Baruch K (2014) The resolution of neuroinflammation in neurodegeneration: leukocyte recruitment via the choroid plexus. EMBO J 33(1):7–22. doi:10.1002/embj.201386609

34. Schwarzmaier SM, de Chaumont C, Balbi M, Terpolilli NA, Kleinschnitz C, Gruber A, Plesnila N (2016) The formation of microthrombi in parenchymal microvessels after traumatic brain injury is independent of coagulation factor XI. J Neurotrauma 33:1634–1644. doi:10.1089/neu.2015.4173

35. Shechter R, London A, Schwartz M (2013) Orchestrated leukocyte recruitment to immune-privileged sites: absolute barriers versus

educational gates. Nat Rev Immunol 13:206–218. doi:10.1038/nri3391

36. Shechter R, Miller O, Yovel G, Rosenzweig N, London A, Ruckh J, Kim KW, Klein E, Kalchenko V, Bendel P et al (2013) Recruitment of beneficial M2 macrophages to injured spinal cord is orchestrated by remote brain choroid plexus. Immunity 38:555–569. doi:10.1016/j.immuni.2013.02.012

37. Steffen BJ, Butcher EC, Engelhardt B (1994) Evidence for involvement of ICAM-1 and VCAM-1 in lymphocyte interaction with endothelium in experimental autoimmune encephalomyelitis in the central nervous system in the SJL/J mouse. Am J Pathol 145:189–201

38. Tietz S, Engelhardt B (2015) Brain barriers: crosstalk between complex tight junctions and adherens junctions. J Cell Biol 209:493–506. doi:10.1083/jcb.201412147

39. Tymianski M (2015) Neuroprotective therapies: preclinical reproducibility is only part of the problem. Sci Transl Med 7:299. doi:10.1126/scitranslmed.aac9412

40. Umekawa T, Osman AM, Han W, Ikeda T, Blomgren K (2015) Resident microglia, rather than blood-derived macrophages, contribute to the earlier and more pronounced inflammatory reaction in the immature compared with the adult hippocampus after hypoxia-ischemia. Glia 63:2220–2230. doi:10.1002/glia.22887

41. Urra X, Miro F, Chamorro A, Planas AM (2014) Antigen-specific immune reactions to ischemic stroke. Front Cell Neurosci 8:278. doi:10.3389/fncel.2014.00278

42. Victora GD, Schwickert TA, Fooksman DR, Kamphorst AO, Meyer-Hermann M, Dustin ML, Nussenzweig MC (2010) Germinal center dynamics revealed by multiphoton microscopy with a photoactivatable fluorescent reporter. Cell 143:592–605. doi:10.1016/j.cell.2010.10.032

43. Waggott D, Chu K, Yin S, Wouters BG, Liu FF, Boutros PC (2012) NanoStringNorm: an extensible R package for the pre-processing of NanoString mRNA and miRNA data. Bioinformatics 28:1546–1548. doi:10.1093/bioinformatics/bts188

44. Wang Q, Tang XN, Yenari MA (2007) The inflammatory response in stroke. J Neuroimmunol 184:53–68. doi:10.1016/j.jneuroim.2006.11.014

45. Wilson EH, Weninger W, Hunter CA (2010) Trafficking of immune cells in the central nervous system. J Clin Investig 120:1368–1379. doi:10.1172/JCI41911

46. Wolburg K, Gerhardt H, Schulz M, Wolburg H, Engelhardt B (1999) Ultrastructural localization of adhesion molecules in the healthy and inflamed choroid plexus of the mouse. Cell Tissue Res 296:259–269

47. Zhou W, Liesz A, Bauer H, Sommer C, Lahrmann B, Valous N, Grabe N, Veltkamp R (2013) Postischemic brain infiltration of leukocyte subpopulations differs among murine permanent and transient focal cerebral ischemia models. Brain Pathol 23:34–44. doi:10.1111/j.1750-3639.2012.00614.x